

# Comparison of time-varying system identification methods to assess joint impedance

by

## Sven Kraaijevanger

to obtain the degree of Master of Science  
at the Delft University of Technology,  
to be defended publicly on Tuesday September 18, 2018 at 2:30 PM.

Student number:	4154053		
Project duration:	September 1, 2017 – September 18, 2018		
Thesis committee:	Dr. ir. A.C. Schouten,	Chairman	BME, TU Delft
	Dr. ir. W. Mugge,	Supervisor	BME, TU Delft
	Ir. M. van de Ruit,	Daily supervisor	BME, TU Delft
	Dr. M. Kok,	External member	DCSC, TU Delft

An electronic version of this thesis is available at <http://repository.tudelft.nl/>.



# Acknowledgements

I would like to thank my supervisors Alfred Schouten and Winfred Muge for their guidance through the graduation process. Your always valuable feedback has improved my research abilities, and your advice has made my thesis to a success. The many meetings were serious, but I always left with a smile.

I would like to thank my daily supervisor, Mark van de Ruit, for providing me with technical support and directing me in the right directions. You always invited me to ask as many questions as I liked, taught me a lot about presenting my work and the importance of the smaller details.

I would like to thank Eric Perrault for inviting me to his Neuromuscular Control and Plasticity Lab in the Shirley Ryan AbilityLab in Chicago. Seeing all the patients around me in the hospital has been a great motivator for my work. Furthermore I would like to thank you for providing the means to build the mechanical device needed for the experiments.

I would like to thank my supervisor in Chicago, Daniel Ludvig, for teaching me a great deal about system identification. Your seemingly endless amount of knowledge was very inspiring. You could answer any question I had by asking me a question in return and making me realize I already knew the answer.

I would like to thank Tim Haswell, the engineer of the Lab. You were always very patient to help me select the right parts, teach me how to use the machinery, and assemble the device.

I would like to thank Costa, Emma, Hongchul, Michel, Rosalind, and Will, the members of the lab, for accepting me in the lab from the start. It was great to take a small peak into your projects and broadening my interests.

I would like to thank my friends and family. Your love and support has provided a solid foundation to help me get to where I am today.

I would like to thank Boaz for providing me with the necessary distractions during the writing of my thesis. You helped keep my sanity with our late night Hunt sessions.

I would like to thank my girlfriend, Ruby, for always being there for me. Even though you did not always understand what I was telling you, you patiently listened to my gibberish. You motivated me to work on my project and made me feel more confident about my work.

Sven Kraaijevanger

Leiden  
September 7, 2018

# Acronyms

<b>BME</b>	BioMechanical Engineering
<b>DCSC</b>	Delft Center for Systems and Control
<b>FRF</b>	Frequency Response Function
<b>IRF</b>	Impulse Response Function
<b>LPV</b>	Linear Parameter Varying method
<b>KBR</b>	Kernel Based Regression method
<b>eIRF</b>	Ensemble Impulse Response Function Method
<b>bIRF</b>	Basis Impulse Response Function Method
<b>SDS</b>	Short Data Segment Method
<b>ESM</b>	Ensemble Spectral Method
<b>mESM</b>	Multitaper Ensemble Spectral Method
<b>SNR</b>	Signal-to-Noise Ratio
<b>FGWN</b>	Filtered Gaussian White Noise
<b>PRBS</b>	Pseudorandom Binary Sequence
<b>EMG</b>	Electromyographic
<b>MVC</b>	Maximum Voluntary Contraction

CONTENTS

<b>I</b>	<b>Introduction</b>	5	<b>VII</b>	<b>Conclusions</b>	18
I-A	Identification of joint impedance . . . . .	5	<b>References</b>		18
I-B	Thesis objective . . . . .	5	<b>VIII</b>	<b>Appendix</b>	20
<b>II</b>	<b>Time-varying system identification methods</b>	6	VIII-A	Time-varying system identification methods . . . . .	20
II-A	Linear parameter varying . . . . .	6	VIII-A1	LPV . . . . .	20
II-B	Kernel based regression . . . . .	6	VIII-A2	eIRF . . . . .	20
II-C	Ensemble impulse response function . . . . .	6	VIII-A3	bIRF . . . . .	20
II-D	Basis impulse response function . . . . .	7	VIII-A4	SDS . . . . .	20
II-E	Short data segments . . . . .	7	VIII-A5	ESM & mESM . . . . .	21
II-F	Ensemble spectral method . . . . .	7	VIII-A6	KBR . . . . .	21
<b>III</b>	<b>Simulation study</b>	7	VIII-B	Extraction and mapping of true stiffness of mechanical variable stiffness device . . . . .	22
III-A	Model . . . . .	7	VIII-B1	Time-invariant trials . . . . .	22
III-B	Simulations . . . . .	8	VIII-B2	Stiffness calculation . . . . .	22
III-C	Performance analysis . . . . .	8	VIII-C	Identification parameters of time-varying methods . . . . .	23
III-D	Results of simulation study . . . . .	9			
III-E	Main observations simulation study . . . . .	10			
<b>IV</b>	<b>Experimental study variable stiffness device</b>	10			
IV-A	Variable stiffness device . . . . .	10			
IV-B	Method of experimental study variable stiffness device . . . . .	11			
IV-C	Results of experimental study mechanical system . . . . .	11			
IV-D	Main observations mechanical experiment . . . . .	13			
<b>V</b>	<b>Experimental study human joint</b>	13			
V-A	Subjects . . . . .	13			
V-B	Experimental setup . . . . .	14			
V-C	Measurement protocol . . . . .	14			
V-D	Data analysis . . . . .	14			
V-E	Results of experimental study human joint . . . . .	14			
V-F	Main observations of experimental study human joint . . . . .	15			
<b>VI</b>	<b>Discussion</b>	15			
VI-A	Signal-to-noise ratio . . . . .	15			
VI-B	Number of samples . . . . .	16			
VI-C	Time-variation . . . . .	16			
VI-D	Perturbation signal . . . . .	16			
VI-E	True stiffness of the mechanical system . . . . .	17			
VI-F	Limitations . . . . .	17			
VI-G	Methods . . . . .	17			

# Comparison of time-varying system identification methods to assess joint impedance

Sven Kraaijevanger, Delft University of Technology, The Netherlands

**Abstract**—Joint impedance describes the dynamic resistance of a joint in response to position perturbations. Joint impedance is known to vary nonlinearly during movement caused by varying joint angle and muscle activation. The nonlinear behaviour can be described using linear time-varying models under certain assumption. Recently a number of time-varying system identification algorithms to estimate joint impedance have been developed. System identification algorithms are typically validated in simulation. These algorithms have not yet been compared using the same simulated data or validated using real experimental data in this application. In this study the algorithms are assessed on their ability to estimate joint stiffness using three data sets. The first data set is from a simulation model representing joint dynamics with time-varying stiffness and damping. The second data set is from a mechanical variable stiffness device. A mapping of the true stiffness of the device was extracted by interpolating the estimated stiffness of time-invariant trials. The last data set is real experimental data from a human ankle with varying contraction levels to which small position perturbations were applied. The simulation study and the experimental mechanical study suggest that when estimating stiffness the linear parameter varying (LPV) method has a bias, the kernel based regression (KBR) method overall has the highest error, the ensemble impulse response function (eIRF) method needs many repetitions, the basis impulse response function (bIRF) method is able to achieve the lowest error, the short data segment (SDS) method is the most robust to different perturbation signals, and the ensemble spectral methods (ESM and mESM) are able to achieve reasonable results. The results of the experimental human study show that the estimated stiffness by the ensemble and short data segment methods have a trend similar to that of the EMG signal, albeit with different offsets. The bIRF, SDS, ESM and mESM make a reasonable compromise between smoothness and required repetitions.

**Keywords**—Joint impedance, System identification, Time-varying systems, Human motor control

## I. INTRODUCTION

### A. Identification of joint impedance

The mechanical properties of our limbs enable and constrain our ability to interact with the physical world. Understanding how the mechanical properties are regulated during natural movement is critical for understanding the ability to interact with the world and how they are compromised following injury. Joint impedance is comprised of the combination of intrinsic and reflexive properties [1]. The intrinsic properties originate from the inertial, viscous, and elastic properties of the tissue surrounding the joint which can be modulated by voluntary muscle contractions. The reflexive properties are attributed to the involuntary muscle contractions in response to perturbations [2].

The quantification of joint impedance during motor tasks contributes to the better understanding of the control and

physiology of the neuromuscular system. The mechanical properties of a limb can be quantified using estimates of joint impedance, the dynamic relationship between the rotation and torque acting around a joint. The quantification of joint impedance has multiple medical applications. Measuring joint impedance during functional tasks can be used for the design of active prostheses to make them interact with the environment naturally [3], [4] and will enhance the mobility of the users [5], [6], [7]. Furthermore, estimates of joint impedance can be used to monitor the treatment of movement disorders.

To quantify joint impedance, system identification methods are employed which make use of experimentally obtained position and torque measurements of a joint during perturbations. Joint impedance has been studied extensively during static postural tasks over the past decades using Linear Time-Invariant (LTI) methods [2], [8], [9], [10]. These LTI methods only produce a local estimate of joint impedance and are thus only valid for an operational point. Joint impedance is known to vary nonlinearly which has multiple mechanical and physiological causes such as joint angle and muscle activation [1], [11], [12].

Fewer studies have quantified joint impedance over the joint's nonlinear range. A major reason for the limited number of studies is the challenge with estimating impedance over an operating range where the identified system can no longer be linearized. Nonlinear time-invariant systems can be described by linear time-varying models, as the nonlinear behaviour can be treated as if it were caused by the change of time. This allows for the employment of linear time-varying methods for the identification of nonlinear time-invariant systems.

### B. Thesis objective

Recently a number of methods have been developed to quantify joint impedance during movement (Subspace [13], [14], [15], Prediction Error [16], and Nonparametric [17], [18], [19]). All these methods have proven to be accurate when validated with simulated data, however, the simulations have been conducted under different assumptions of signal-to-noise ratio (SNR) and signal properties. The methods have not yet been compared using the same simulated data allowing for a true comparison. Furthermore, the performance when working with experimental data has not been thoroughly tested for all methods.

The objective of this thesis is to assess the accuracy and robustness of seven time-varying joint impedance estimation algorithms. These seven algorithms are tested because they were available to the author, either through the university or the internet. The assessment of the accuracy and robustness will be done using three data sets:

- The first data set is simulation data, where the true underlying values of impedance are known and the signal-to-noise ratio can be easily controlled. This first data set will be used to confirm that the algorithms are capable of producing accurate estimates of the impedance. Furthermore, the lower boundary of signal-to-noise ratio for which the algorithms can still produce reliable estimates can be determined.
- The second data set is experimental data from a mechanical system. A mechanical device with a known time-varying impedance has been designed and built. The impedance of the mechanical device was estimated with equipment traditionally used to quantify joint impedance. The purpose of this second data set will be to validate the performance of the algorithm with real experimental data. This validation has never been done before and is a novel contribution to the field.
- The final data set will be real experimental data collected from humans during a postural task with time-varying joint torque. It is not possible to assess the accuracy of the estimates generated by the algorithm for this final data set, as the true time-varying values of the human joint impedance are not known. However, the values can be compared to estimates from linear time-invariant methods. Furthermore, this final data set will allow the comparison of the estimated joint impedance of the algorithms on human data.

## II. TIME-VARYING SYSTEM IDENTIFICATION METHODS

Three main system identification classes exist; Subspace, Prediction Error and Nonparametric methods. In this section first the three main system identification classes will be described. Then the concepts of the seven algorithms compared in this paper will be explained. The seven algorithms are classified in Table I. The corresponding mathematics of the algorithms can be found in Appendix VIII-A. The parameters used in the system identification methods can be found in Appendix VIII-C.

- During subspace identification, a Hankel matrix is created from the input and output data. From this Hankel matrix the singular values are used to derive the order of the system and a subspace of the system [20]. The subspace contains the essential data and the system can be reconstructed by performing a similarity transformation. The system is described using a state-space model where the time-variation is represented by time-dependent system matrices of the state-space model.
- During prediction error methods, the system is modelled parametrically. A cost function is expressed in terms of the observed and predicted model output based on the given input. The time-variation is represented by time-varying parameters in the model. The system can be described by input-output model structures or state-space models.
- During nonparametric estimation the system is described using a Frequency Response Function (FRF)

or Impulse Response Function (IRF). In the time-domain the correlation of the input and output data is used to compute the IRF/FRF, where in the frequency domain spectral densities of the input and output data are used. The time-variation is represented by computing a response function for every time step.

TABLE I. CLASSIFICATION OF TIME-VARYING METHODS INVESTIGATED IN THIS THESIS.

Class	Method	Acronym
Subspace	Linear Parameter Varying [13]	LPV
Prediction Error	Kernel Based Regression [21]	KBR
Non-Parametric	Ensemble Impulse Response Function [22]	eIRF
	Basis Impulse Response Function [17]	bIRF
	Short Data Segments [18]	SDS
	Ensemble Spectral method*	ESM
	Multitaper Ensemble Spectral method*	mESM

\*The ESM and mESM by Alfred C. Schouten are still in preparation at this time, and are thus not referenced.

### A. Linear parameter varying

The linear parameter varying (LPV) method makes use of the assumption that there is a known scheduling function. The estimated system matrices of the state-space model are multiplied by the scheduling function to describe the time-varying behaviour. The method is based on an existing LPV method [23]. However, this method is unable to describe improper systems, e.g. experiments done with position perturbations. This is overcome by implementing the generalized state-space system description from a time-invariant method described in [24]. The causal and anti-causal description are combined into the non-causal form, allowing the use of position perturbations. [13]

### B. Kernel based regression

The kernel based regression (KBR) method assumes that the input and output signals can be explained by a linear differential equation. The parameters of the differential equation vary with time, explaining the time-varying behaviour. The time-varying parameters are described by a set of basis functions, in this case a set of radial basis function kernels, causing the smooth behaviour. The coefficients of the differential equation are estimated in the frequency domain via a kernel-based regression. The error between the measured output and predicted output is minimized iteratively, as it concerns a non-convex problem. The kernel can be tuned to determine the smoothness of the time-variation and the amount of regularization that is applied. [21]

### C. Ensemble impulse response function

Ensemble methods make use of the assumption that each realization has the same experimental and time-varying conditions, as can be seen in Fig. 1. The assumption that the system

and experimental conditions do not change across realizations allows for the application of time-invariant identification techniques for each time step. The ensemble impulse response function (eIRF) method makes use of this assumption. For each time step during the repeated movement an impulse response function is calculated from the realizations. A downside of this method is that it requires many realizations to make an accurate estimate of the impulse response functions. [22]

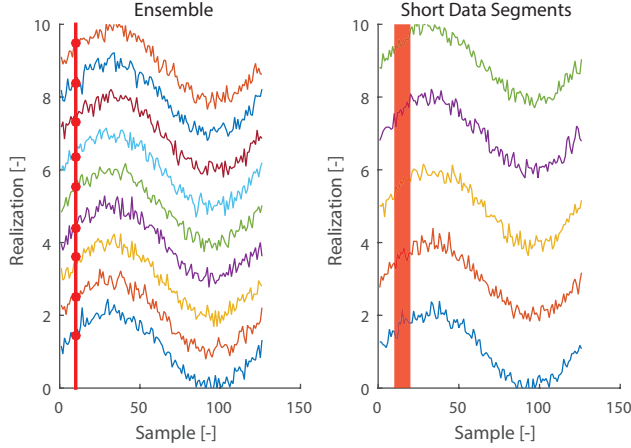


Fig. 1. Graphical representation of ensemble (left) and short data segments (right) methods. Ensemble methods assume that for each realization the time-variation is the same for each point in time (red line). Short data segment methods not only assume that for each realization the time-variation is the same for each point in time, but also for a small window (red bar) surrounding the point in time, averaging over more data and thus needing less data.

#### D. Basis impulse response function

The basis impulse response function (bIRF) method makes use of the same principle as the eIRF method, creating a time-varying impulse response function from ensemble data. After the time-varying impulse response function has been calculated, it is approximated by a linear combination of basis functions. The basis functions create smooth time-varying behaviour, which reduces the effect of noise on the estimate. Less realizations of the movement are needed in comparison to the eIRF. [17]

#### E. Short data segments

The (short data segments) SDS method is again very similar to the eIRF method. Here the assumption is made that not only the realizations have the same time-variation for each time step in each realization, but also for a small window surrounding this time step, see Fig. 1. The impulse response function is thus computed using a sliding window over the whole time variation, effectively using each point multiple times for the estimate. Therefore for each point in the time-variation more samples are used to calculate the impedance when compared to the eIRF method, reducing the effects of noise. The size of the window is a trade-off between the smoothness of the estimate and the amount of noise being rejected. [18]

#### F. Ensemble spectral method

The ensemble spectral method (ESM) and multitaper ensemble spectral method (mESM) are also making use of short

data segments. For each realization and for each point in time the auto- and cross-spectral density are computed using a small window surrounding the point in time. For each point in time the spectral densities are Welch averaged over the realizations. The averaged cross-spectral densities are then divided by the averaged auto-spectral densities to compute the mean FRF for each point in time. The combined FRFs create a time-varying non-parametric description of the system. The difference between the ESM and mESM is that before calculating the spectral densities smoothing is applied. For the ESM a Hanning window is applied [25]. For the mESM method the multitaper method is applied [26].

### III. SIMULATION STUDY

#### A. Model

A time-varying causal open-loop mass-spring-damper system as shown in Fig. 2a was simulated. The simulation represents an experimental setup where a human subject performs a force task while position perturbations are applied. The position perturbations  $u$  are applied through a manipulator, and the torque responses  $y$  are measured. The human typically controls the time-varying torque using visual feedback.

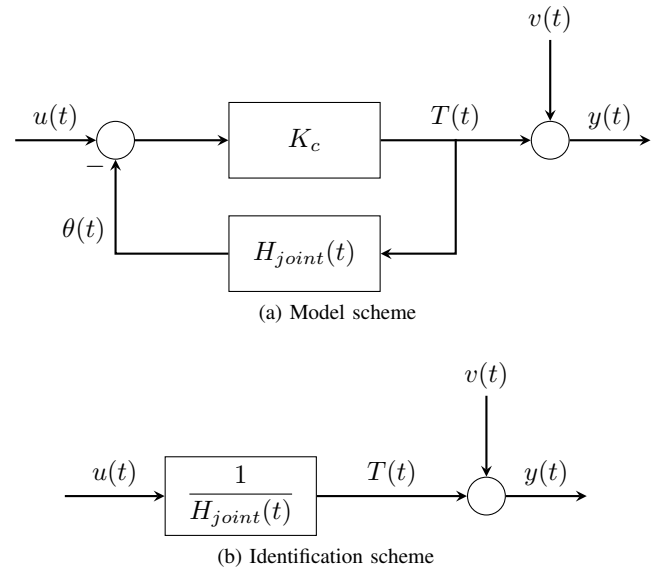


Fig. 2. Schematic representation of the (a) time-varying causal simulation model and (b) identification scheme following Equation (3).  $u(t)$ : angular input perturbation,  $T(t)$  true output torque,  $y(t)$ : measured output torque,  $v(t)$ : measurement noise,  $\theta(t)$ : joint angle,  $H_{joint}(t)$ : time-varying joint dynamics, and  $K_c$ : manipulator gain.

The simulations were carried out using Simulink (The Mathworks Inc.). Mathematically the model is represented as follows:

$$y(t) = \frac{K_c}{1 + K_c H_{joint}(t)} u(t) + v(t) \quad (1)$$

$$= \frac{1}{\frac{1}{K_c} + H_{joint}(t)} u(t) + v(t) \quad (2)$$

Where  $u(t)$  is the angular input perturbation,  $y(t)$  is the measured output torque,  $v(t)$  is the measurement noise,  $\theta(t)$

is the joint angle,  $H_{joint}(t)$  contains the time-varying joint dynamics, and  $K_c$  is the manipulator gain.

The system is in closed-loop, however the gain of the manipulator  $K_c$  was set to 20000 causing the system to approximate an open-loop system as described in Equation (3). This allowed for the usage of an open-loop identification scheme as can be seen in Fig. 2b.

If:

$$K_c \gg 0$$

Then:

$$y(t) = \frac{1}{H_{joint}(t)}u(t) + v(t) \quad (3)$$

The measurement noise  $v(t)$  is modelled as Gaussian white noise low-pass filtered at 40Hz using a 2<sup>nd</sup> order Butterworth filter. The joint dynamics are modelled as a second-order model with a time-varying stiffness and damping represented in the following equation:

$$T(t) = I \frac{d^2\theta(t)}{dt^2} + B(t) \frac{d\theta(t)}{dt} + K(t)\theta(t) \quad (4)$$

where  $T(t)$  is the torque acting on the joint,  $\theta(t)$  is the angle of the joint,  $I$  is the inertia of the joint, and  $B(t)$  and  $K(t)$  are the time-varying joint viscosity and stiffness, respectively. This is a common representation of joint impedance [18]. In the simulation the inverse of joint impedance, joint admittance, was used in order for the simulation to be causal. In the Laplace domain joint admittance is represented as follows:

$$H_{joint}(s, t) = \frac{\Theta(s)}{T(s)} = \frac{1}{Is^2 + B(t)s + K(t)} \quad (5)$$

where  $H_{joint}$  is joint admittance,  $\Theta(t)$  and  $T(s)$  are the input angle and the output torque in the Laplace domain, respectively and  $s$  is the Laplace operator.

The inertia  $I$  of the simulated joint was set to be 0.02 kgm<sup>2</sup>. The joint viscosity was varied with time using a triangle wave between 1.2 and 3.2 Nms/rad and the stiffness was varied using a square wave between 50 and 150 Nm/rad. Both the damping and the stiffness varied with a constant frequency of 1 Hz. A 1Hz time-variation was chosen as the frequency of human gait lies between 0.5Hz and 2Hz. The varying stiffness and damping is visualized in Fig. 3. These time-varying properties were chosen to test the limits of the algorithms. The abrupt changes in dynamics will provide information on how fast the algorithms are able to track changes.

### B. Simulations

The simulations were run using a fixed time step of 0.001s. The simulation time, perturbation signal, SNR, and time-variation were varied systematically. This is summarized in Table II.

The three position perturbation signals used are:

- A Gaussian white noise signal (FGWN) to which a 2<sup>nd</sup> order low-pass Butterworth filter was applied at 5Hz. [18]

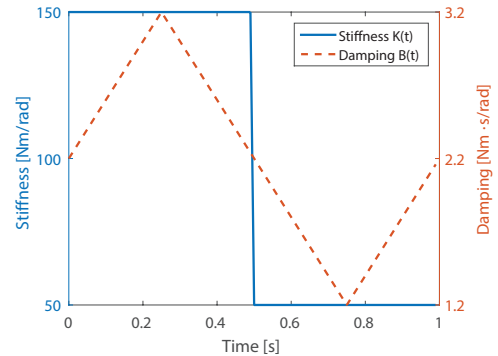


Fig. 3. Visual representation of time-varying stiffness (solid) and damping (dashed).

TABLE II. VARYING CONDITIONS USED IN THE SIMULATIONS.

	Conditions			
Perturbation signal	FGWN	PRBS	Multisine	
Simulation time [s]	25	<u>50</u>	100	200 400
SNR [dB]	-10	<u>0</u>	10	20
Time-variation	-	B	<u>K</u>	KB

Where “-” is no time-variation, B is time-varying damping, K is time-varying stiffness, and KB is time-varying stiffness and damping. The underlined and bold conditions define the baseline conditions used in Table III to expose the effects of the varying conditions independently.

- A pseudorandom binary sequence (PRBS) with a switching rate of 147ms. [18]
- A multisine signal containing the following frequencies: [0.1:0.8:20] Hz. [27]

All three input signals were generated at 1000Hz and low-pass filtered using a 4<sup>th</sup> order Butterworth filter at 40Hz and then scaled to have the same standard deviation. The variance of the noise  $v(t)$  was scaled to control the SNR of the simulations.

The simulation time was varied between 25, 50, 100, 200, and 400 seconds. To study the effect of noise four SNR levels were simulated (-10, 0, 10, and 20 dB). The time-varying dynamics were varied between a time-invariant system, only varying stiffness, only varying damping, and vary both stiffness and damping.

All combinations of varying perturbation signals, simulation time, SNRs and time-variations were simulated leading up to a total of 240 simulations. Before using the system identification algorithms, the data were decimated to 100Hz to reduce the amount of computational memory needed. The simulation still needed to run at 1000Hz to make sure the simulation did not become unstable.

### C. Performance analysis

The quality of the estimates was assessed on their ability to estimate the stiffness of the system. The stiffness parameter was chosen because no assumption had to be made on the

order of the system. The root mean square error (RMSE) of the stiffness is calculated, Equation (6). This is then normalized to the root mean square (RMS) of the stiffness so the results are expressed as a percentage error, Equation (7).

$$RMSE(\hat{K}) = \sqrt{\sum_{i=1}^N \frac{(K_i - \hat{K}_i)^2}{N}} \quad (6)$$

$$\%Error = 100 \left( \frac{RMSE(\hat{K})}{RMS(K)} \right) \% \quad (7)$$

where  $RMSE(\hat{K})$  is the RMSE of the stiffness,  $K_i$  and  $\hat{K}_i$  are the true and estimated stiffness at time step  $i$  respectively, and  $N$  is the total number of samples. When  $\hat{K}$  perfectly follows  $K$  Equation (6) will be equal to zero, resulting in a 0% error. When  $\hat{K}$  is constant, e.g. no time-variation, Equation (7) will result in an error of approximately 100%, given that the algorithm is correct on average.

#### D. Results of simulation study

The results of the simulations are summarized in Table III. To summarize the results for each perturbation signal the median of the error of all simulations with the respective perturbation signal was calculated, also displayed in Fig. 4. The median was chosen, because for some conditions the LPV method would become unstable and would get a very high error which would dominate the average.

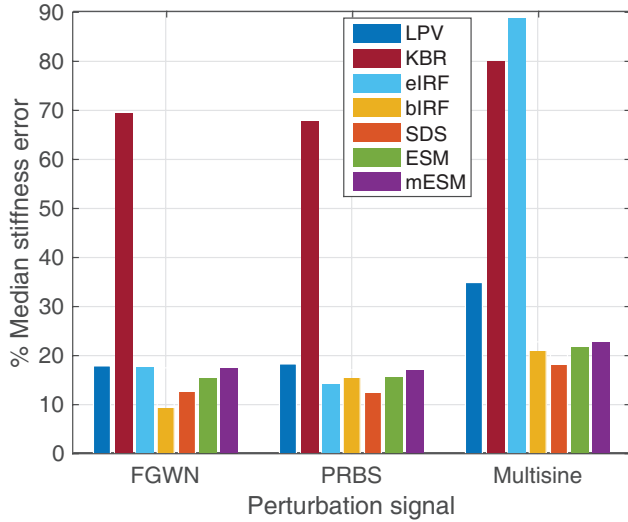


Fig. 4. Bar plot of the median error of the estimated stiffness in the simulation study for each algorithm for each perturbation signal.

A visual representation of the estimated stiffness is shown in Fig. 5. The LPV method shows a similar shape as the varying stiffness, with a small offset. The KBR method is able to track the right frequency and amplitude of the varying stiffness for the FGWN perturbation, albeit very smooth. The eIRF method shows a highly noisy estimate of the stiffness. This noisy result, however, is for just 50 repetitions while this method typically needs hundreds of repetitions to achieve an

TABLE III. RESULTS OF SIMULATION STUDY, NORMALIZED ERROR OF ESTIMATED STIFFNESS [%].

		Normalized error of stiffness [%]							
		LPV	KBR	eIRF	bIRF	SDS	ESM	mESM	
FGWN	Simulation time [s]	25	16.4	41.2	117.7	14.8	23.6	23.1	23.1
		<b>50</b>	<b>14.3</b>	<b>41.7</b>	<b>40.5</b>	<b>11.2</b>	<b>17.9</b>	<b>20.3</b>	<b>23.1</b>
		100	16.6	40.2	26	10.8	14.3	17.3	22
		200	-	-	17.7	9.4	13.2	16	18.4
	SNR [dB]	-10	15.3	74.5	95.9	28.1	29.9	19.3	21
		<b>0</b>	<b>14.3</b>	<b>41.7</b>	<b>40.5</b>	<b>11.2</b>	<b>17.9</b>	<b>20.3</b>	<b>23.1</b>
		10	14.2	34.5	15.3	9.6	13.5	16.3	18.7
	Time-variation	N	16.1	35.2	41.5	10.4	10.4	8.9	10.1
		B	14.8	28	37.2	6.7	9.7	12	13.5
		<b>K</b>	<b>14.3</b>	<b>41.7</b>	<b>40.5</b>	<b>11.2</b>	<b>17.9</b>	<b>20.3</b>	<b>23.1</b>
		KB	22.5	41.6	40.2	11.8	15.7	17.3	18.1
	Median		17.9	70.7	17.4	9.3	12.5	15.3	17.5
PRBS	Simulation time [s]	25	16.8	34.1	65	18	15.6	16.9	22.7
		<b>50</b>	<b>16.3</b>	<b>34.5</b>	<b>30.5</b>	<b>16.1</b>	<b>13.9</b>	<b>15.3</b>	<b>21.9</b>
		100	17.8	34.9	20.1	16.2	13.6	15.9	22.3
		200	-	-	15	15.9	13.7	16.4	19.4
	SNR [dB]	-10	19.2	66.3	84.6	25.7	24.3	20.1	25.4
		<b>0</b>	<b>16.3</b>	<b>34.5</b>	<b>30.5</b>	<b>16.1</b>	<b>13.9</b>	<b>15.3</b>	<b>21.9</b>
		10	16	28.2	11.1	15.1	12.5	15.5	18.8
	Time-variation	N	13.5	25.3	32.3	13.8	6.6	6.1	6.2
		B	14.7	25.4	32.9	13.8	6.6	6	6
		<b>K</b>	<b>16.3</b>	<b>34.5</b>	<b>30.5</b>	<b>16.1</b>	<b>13.9</b>	<b>15.3</b>	<b>21.9</b>
		KB	18.3	34.5	30.8	16.1	13.9	15.3	22
	Median		18.3	67.6	13.9	15.3	12.3	15.6	17.1
Multisine	Simulation time [s]	25	23.1	48.8	108.4	21.2	24.5	20.8	23.8
		<b>50</b>	<b>18.5</b>	<b>48.2</b>	<b>97</b>	<b>22.8</b>	<b>20.8</b>	<b>22.5</b>	<b>20.6</b>
		100	18.8	<b>48.2</b>	93.3	21.5	16.4	22.5	21.5
		200	-	-	93.3	21.1	16.4	23	21.7
	SNR [dB]	-10	27.4	98.1	132.7	31.1	58.5	54.4	47.5
		<b>0</b>	<b>18.5</b>	<b>48.2</b>	<b>97</b>	<b>22.8</b>	<b>20.8</b>	<b>22.5</b>	<b>20.6</b>
		10	18.7	37.6	87.9	22	18.8	21.5	23.8
	Time-variation	N	37	34.3	103.6	24.4	20.6	19.5	22
		B	32.7	34.7	125.6	25.9	17.7	17	21.2
		<b>K</b>	<b>18.5</b>	<b>48.2</b>	<b>97</b>	<b>22.8</b>	<b>20.8</b>	<b>22.5</b>	<b>20.6</b>
		KB	26.1	45.9	91.9	23.1	19.7	23.2	26
	Median		34.9	79.9	88.6	20.9	18.1	21.7	22.8

For each type of perturbation signal a baseline was defined to study the effects of the conditions while keeping all other conditions constant. The baseline used was a simulation time of 50 seconds, a SNR of 0 dB, and variation of only the stiffness. The results of the baseline are indicated in bold. A visual representation of the results can be seen in Fig. 5. Note that not all the results of the 240 simulations are displayed. The LPV and KBR method required too much memory to make an estimate for a certain amounts of samples. These failed estimates are marked in the table with a "-".

accurate result. The bIRF, SDS, ESM, and mESM show a reasonable estimate of the stiffness.

The lowest median error for the LPV method is 17.9% when used with FGWN perturbations. The estimate of joint stiffness did not improve with longer simulations. It did improve with a higher SNR. The time-varying conditions do

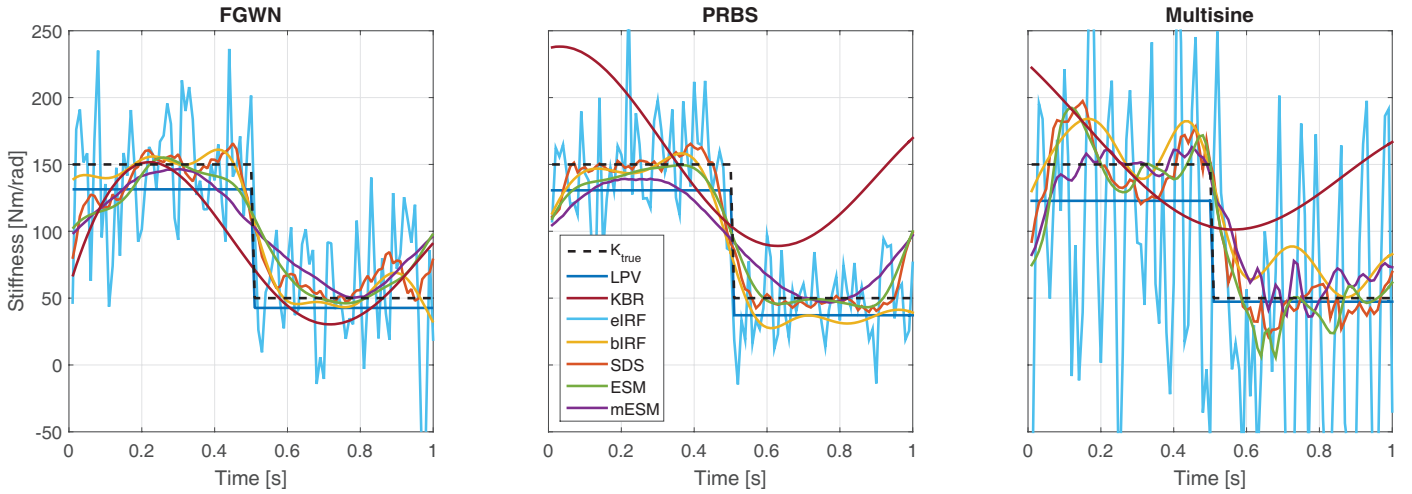


Fig. 5. Visual representation of the estimated stiffness in the simulation study for each perturbation signal and the baseline conditions; 50s simulation time, SNR of 0dB, and only varying stiffness. The true stiffness is shown as a black dashed line.

not have an influence on the estimates.

The lowest median error for the KBR method is 67.7% when used with PRBS perturbations. This is the highest overall median error when estimating stiffness. The estimate of joint stiffness did not improve with longer simulations. It did improve with a higher SNR. The algorithm was able to make a better estimate of the stiffness when it was not varying.

The lowest median error for the eIRF method is 13.9% when used with PRBS perturbations. The estimate of joint stiffness improved the most with longer simulations and a higher SNR. The time-varying conditions do not have an influence on the estimates.

The lowest median error for the bIRF method is 9.3% when used with FGWN perturbations. The estimate of joint stiffness improved with longer simulations and a higher SNR. The time-varying conditions do not have an influence on the estimates.

The lowest median error for the SDS method is 12.3% when used with PRBS perturbations followed closely by a median error of 12.5% for FGWN perturbations. The estimate of joint stiffness improved with longer simulations and a higher SNR. The algorithm was able to make a better estimate of the stiffness when it was not varying.

The lowest median error for the ESM method is 15.3% when used with FGWN perturbations. The estimate of joint stiffness improved with longer simulations and a higher SNR. The algorithm was able to make a better estimate of the stiffness when it was not varying.

The lowest median error for the mESM method is 17.1% when used with PRBS perturbations. The estimate of joint stiffness improved with longer simulations and a higher SNR. The algorithm was able to make a better estimate of the stiffness when it was not varying.

Overall the performance of the algorithms is similar for both the FGWN and PRBS signal. The estimates with a multisine perturbation structurally have a higher error than the other two input signals.

#### E. Main observations simulation study

- The best results were achieved using FGWN and PRBS perturbations.
- The stiffness estimates improved with longer simulation times for the short data segment methods (SDS, mESM, and ESM) and ensemble methods (eIRF and bIRF).
- The methods that are smoothed due to their algorithm (SDS, ESM, mESM, KBR and, bIRF) had more trouble estimating the abrupt changes of the stiffness.
- The bIRF and short data segment methods seem to make a reasonable trade-off between smoothing and accuracy.
- The error of all methods decreased with a higher SNR, except for the LPV method where the error increased, suggesting that the method has a bias.
- The KBR structurally has the highest error, except for the multisine perturbation where the eIRF has a slightly higher error.
- The eIRF method is the only method to truly track the fast changes as the method calculates joint impedance for each independent time step. However, in order to accurately track the fast changes the method requires hundreds of repetitions.
- The SDS and bIRF perform the best, where SDS is the most robust, bIRF has the lowest median error.
- The ESM and mESM are two very similar methods, however the ESM is able to structurally achieve a lower error than the mESM.

## IV. EXPERIMENTAL STUDY VARIABLE STIFFNESS DEVICE

### A. Variable stiffness device

The variable stiffness device (Fig. 6 and 7) consists of a rod to which two springs are attached at one end (right side),

and to which perturbations are applied to the other end (blue arrow on the left). In the middle of the rod the combination of a rotational and linear bearing acts as a rotational point (red). In the variable stiffness device the actual stiffness of the springs in the system does not change, but rather the rotational point (red) moves, effectively changing the moment arm on either side. This makes that the stiffness on the left outer end of the device changes when the position of the rotational point changes, making it time-varying.

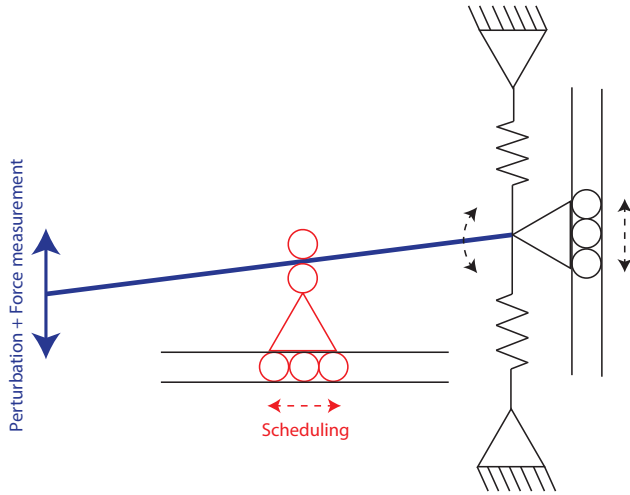


Fig. 6. Schematic of variable stiffness device

The rotational point is actuated using a lead screw driven by a DC motor. The position of the rotational point was measured by a linear potentiometer and controlled using a PID controller running on an Arduino Uno.

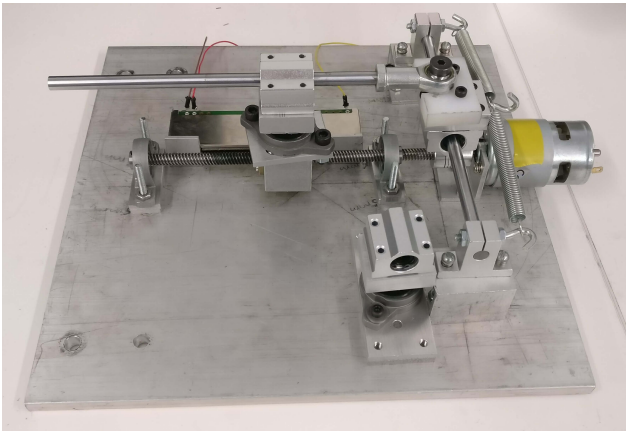


Fig. 7. Photo of the completely assembled variable stiffness device

A mapping of the true stiffness of the mechanical system was extracted by several time-invariant trials over the full range of motion. The estimated stiffness of the time-invariant trials were then interpolated to create a mapping over the full range of motion of the device. This process was repeated for both FGWN and PRBS perturbations. The details of the time-invariant trials and mapping there-off can be found in Appendix VIII-B. The theoretical and estimated stiffness is presented in Fig. 8.

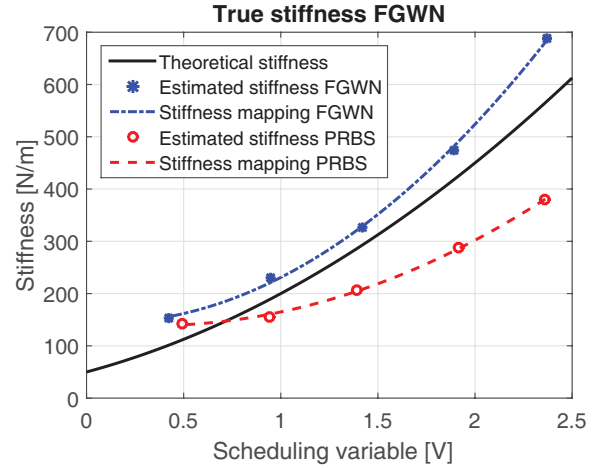


Fig. 8. Theoretical and estimated stiffness interpolated between time-invariant trials for both FGWN and PRBS perturbations.

### B. Method of experimental study variable stiffness device

Perturbations were applied to the variable stiffness device by a linear motor. Position, force, and scheduling variable data was recorded at 2500Hz. For each condition 1000 seconds of data was collected.

A total of eight time-varying experiments were run, testing different perturbation signals and time-varying behaviours. The experimental time used for identification was varied as well, leading up to a total of 40 datasets. The used conditions are displayed in Table IV.

TABLE IV. VARYING CONDITIONS FOR THE MECHANICAL EXPERIMENT.

Experimental time [s]	24	50	100	200	400
Perturbation signal	FGWN			PRBS	
Time-variation	0.5Hz square	0.5Hz sine	1Hz sine	2Hz sine	

The PRBS signal had an amplitude of 5mm and a switching rate of 147 ms. The FGWN signal is white noise signal to which a 2nd order low-pass Butterworth filter was applied at 5Hz and was scaled to have a standard deviation of 2mm. Both signals were low-pass filtered with a 4<sup>th</sup> order Butterworth filter at 40Hz. The amplitude of the time-varying behaviour is the same for all experiments. The collected data were decimated to 100Hz before the identification algorithms were applied.

### C. Results of experimental study mechanical system

Position, torque, and scheduling data are presented in Fig. 9 for both perturbations. The FGWN input had a mean of 0mm with a standard deviation of 20mm. The PRBS input had a mean of 25mm with a standard deviation of 24mm.

All results of the 40 data sets are displayed in Table V. For both perturbation signals the median of the normalized error was calculated.

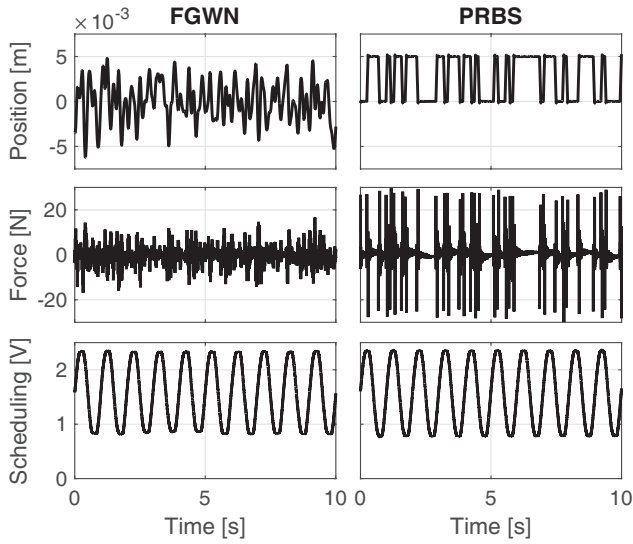


Fig. 9. Visual representation of the input, output, and scheduling of the 1Hz sine wave experiments on the variable stiffness device.

The lowest median error for the LPV method is 25% when used with FGWN perturbation. The algorithm has lower errors with the FGWN perturbation for each condition. The estimate of the stiffness did not improve with longer simulations.

The lowest median error for the KBR method is 41.9% when used with FGWN perturbations. This is the highest overall median error when estimating stiffness. Overall the algorithm performed better with FGWN perturbations for each condition. The estimate of the stiffness did not improve with an increased experimental time. When used with FGWN perturbations the algorithm was able to track the frequency of the time-variation, this was not the case for PRBS perturbations.

The lowest median error for the eIRF method is 15.4% when used with FGWN perturbations. The algorithm obtains better estimates with the FGWN for each condition. The estimate of the stiffness improved with an increased experimental time for all experiments. The results for the PRBS perturbations contain more noise than the results with the FGWN perturbations.

The lowest median error for the bIRF method is 11.7% when used with FGWN perturbations. The algorithm has the lowest error with the FGWN perturbation for each condition. The estimate of the stiffness improved with an increased experimental time for most experiments. The algorithm has the highest error for the 0.5Hz sine time-variation for both perturbation types.

The lowest median error for the SDS method is 12.1% when used with FGWN perturbations, followed closely by the PRBS perturbation with a median error of 12.5%. This algorithm also has the lowest error when used with a PRBS perturbation for all conditions. The estimate of the stiffness improved with an increased experimental time for most experiments. The algorithm has the highest error for the 0.5Hz sine time-variation for both perturbation types.

The lowest median error for the ESM method is 22.6% when used with FGWN perturbations. Overall the algorithm

obtains better estimates with the FGWN perturbations. The estimate of the stiffness improved with an increased experimental time for only some of the experiments. The algorithm has the highest error for the 0.5Hz sine time-variation for both perturbation types.

The lowest median error for the mESM method is 22.8% when used with FGWN perturbation. Overall the algorithm obtains better estimates with the FGWN perturbations. The estimate of the stiffness improved with an increased experimental time for only some of the experiments. The algorithm has the highest error for the 0.5Hz sine time-variation for both perturbation types.

TABLE V. RESULTS OF EXPERIMENTAL MECHANICAL STUDY, NORMALIZED ERROR OF ESTIMATED STIFFNESS DISPLAYED AS % ERROR.

		Normalized error of stiffness [%]							
		LPV	KBR	eIRF	bIRF	SDS	ESM	mESM	
FGWN	0.5Hz square	24	14.5	40.8	60.2	17.2	22.1	48.4	51.4
		50	22.7	39.9	38.4	12.8	12.1	40.6	54.7
		100	20.1	40.8	13.7	11.2	9.2	35.6	43.9
		200	-	-	9.7	9.6	5.7	18.8	21.1
		400	-	-	8.3	8.8	5.6	11.9	14.6
	0.5Hz sine	24	28.2	33.2	98.3	18	23.6	45.8	45.8
		50	21.5	31.2	46.4	12.1	17.9	26.6	22.9
		100	26.3	33.4	22.5	13.9	18.3	24.7	22.4
		200	-	-	24.8	18.2	21	36.4	39.4
		400	-	-	22.6	17.1	20.3	35.4	38.8
	1Hz sine	24	17.7	38.2	48.5	12.1	11.6	16.9	11.4
		50	19.5	41.2	17.9	7.1	10.9	12.5	9.3
		100	24.9	42.9	15	7.2	10.9	21	22.2
		200	-	-	13.3	6.7	10.5	22	25.4
		400	-	-	11.9	6	9.6	29.5	20.5
	2Hz sine	24	17.5	56.7	15.8	21.3	9.2	10	10.1
		50	25.2	56.1	14.6	13.3	12.4	19.6	10.1
		100	23.8	55.1	14.3	9.2	12.1	19.7	22.6
200		-	-	14.	9.1	12.7	23.1	25.2	
400		-	-	13.6	7.6	12.6	19.1	22.7	
Median		25	41.9	15.4	11.7	12.1	22.6	22.8	
PRBS	0.5Hz square	24	33.5	48.6	357.1	26.1	12.4	41.5	47.5
		50	33.4	49.5	48.2	23.6	13.7	40.4	47
		100	35.5	49.6	32.2	23	12	42.6	49.2
		200	-	-	27.8	21.7	12.2	43	50.7
		400	-	-	26.1	21.7	12.7	48.1	52.8
	0.5Hz sine	24	53.1	36.2	161.6	33.1	17.9	59.8	63.4
		50	61.3	38.1	53.3	31.2	17.2	66.3	69.7
		100	64.7	39.3	24.3	32.7	16.3	64.9	68
		200	-	-	15.6	33.9	14.9	66.6	70
		400	-	-	12.1	34.1	14.4	69.9	73.2
	1Hz sine	24	29.7	46.9	50.1	19.5	15.5	39.2	40
		50	29.6	50.1	36.3	19.2	14.2	39	40.5
		100	29.5	46.3	30.7	19.7	12.7	37.8	40
		200	-	-	27	20.4	10.1	39.5	41.8
		400	-	-	25.3	20.7	9.5	41.4	43.8
	2Hz sine	24	33.1	59.5	23.6	24.3	8.9	38.9	40.7
		50	46.4	55.6	22.1	24.3	7.5	37.3	39.9
		100	32.6	57.5	21.4	25.5	6.8	40.7	42.2
200		-	-	19.9	26.4	6.4	41.5	44.5	
400		-	-	19.1	26.9	6.7	44.6	46	
Median		41.3	49.6	26.5	24.3	12.5	41.5	46.5	

The LPV and KBR method required too much memory to make an estimate for certain amounts of samples. This is marked in the table with a "-".

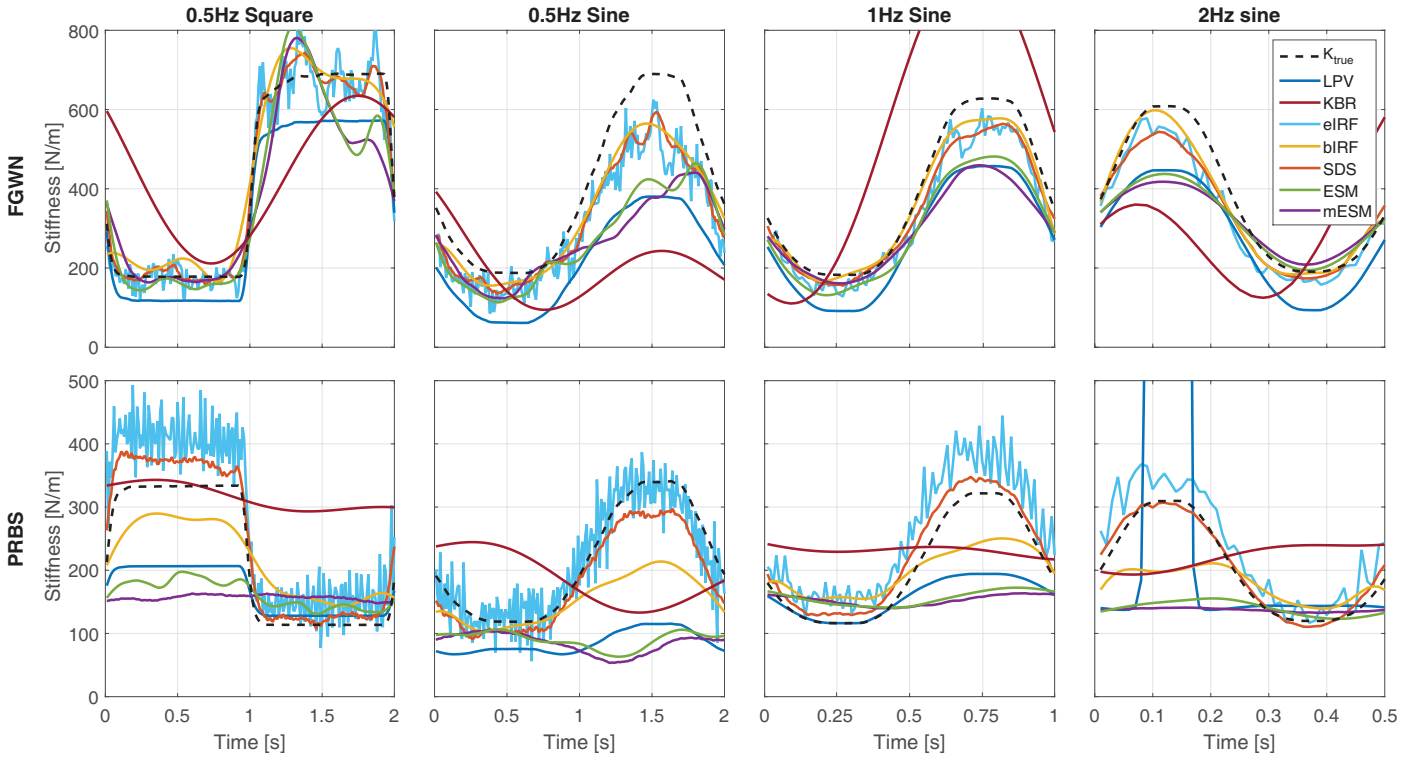


Fig. 10. Visual representation of the estimated stiffness for the mechanical study for each perturbation signal and time-variation. These estimates are made using 100 seconds of data.

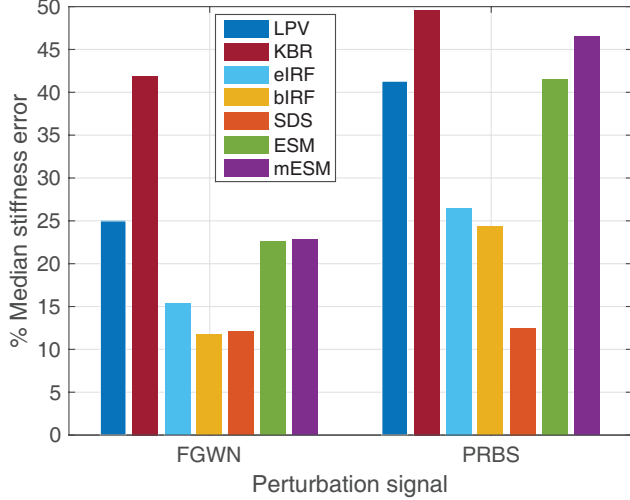


Fig. 11. Visual representation of the median error between the true and estimated stiffness for the mechanical study for both perturbation signals.

#### D. Main observations mechanical experiment

- The mapping of estimated true stiffness have different ranges for the two perturbation signals.
- All methods have a lower median error for FGWN perturbations than for PRBS perturbations, even though the FGWN signal has a lower SNR.
- Results of 0.5Hz sine converged to a different value than the estimated true value.

- The LPV method created a larger error with more data, indicating that it has a bias, similar to the simulation study.
- The KBR method structurally has the highest error, similar to the simulation study.
- The bIRF method is able to achieve the lowest error, but only for the FGWN perturbation, similar to the simulation study.
- The SDS method is the most robust with a low error regardless of perturbation signal, similar to the simulation study.
- The ESM structurally performs better than the mESM, similar to the simulation study.
- The normalized error generally went down with an increased experimental time for short data segment methods and ensemble methods.

## V. EXPERIMENTAL STUDY HUMAN JOINT

### A. Subjects

Six healthy participants (2 men, 4 women),  $24 \pm 1$  years, with no self-reported history of neurological or orthopedic leg problems, participated in the experiment. One participant was left legged, all other participants were right legged, this was self reported. The study was approved by human research ethics committee (HREC) of the Delft University of Technology. All participants provided written informed consent before participating.

## B. Experimental setup

Participants were seated in a car seat and asked to place their left foot on the pedal of a haptic manipulator resembling a car's gas pedal (the 'Achilles' - MOOG, Nieuw-Vennep, the Netherlands), see Fig. 12. The foot of the participant was strapped to the pedal using Velcro to ensure a firm connection to the device. The car seat was adjusted so that the knee of the participant was in an angle of 90 degrees. A screen in front of the participant provided a target trajectory representing the torque the subject had to exert. A cursor provided visual feedback of their current torque levels (0.6Hz low-pass filtered). During all trials the torque on the pedal and position of the pedal were measured, sampled at 1024Hz. Electromyographic (EMG) responses of the gastrocnemius medialis muscle were measured at 1024Hz. The EMG signal was measured using the TMSi Porti7 in a bipolar configuration using Ambu Blue Sensor N silver chloride surface electrodes.



Fig. 12. Picture of a participant attached to the Achilles haptic manipulator.

## C. Measurement protocol

All participants completed 20 trials, 10 trials of two different perturbation signals. Prior to the trials the maximum voluntary contraction (MVC) was determined. During the measurement of the MVC, the backrest of the car seat was removed to ensure that the exerted force was coming from the foot. The backrest was placed back comfortably during the trials. The trials required the participant to apply a varying voluntary torque. The participants were asked to track a 0.5Hz sine wave between 5 and 50% MVC on the screen while ignoring the continuous angular perturbations applied by the ankle manipulator. A frequency of 0.5Hz was chosen as this frequency is controllable by a human and close to the frequency of human gait. Each trial lasted 70s including 5s at the start and end of each trial without perturbations. The participants were allowed 3 practice trials to get used to the perturbations for each perturbation. The two types of perturbation signals used were; A filtered Gaussian white noise (FGWN) signal (5Hz 2<sup>nd</sup> order low-pass Butterworth filtered), and a pseudorandom binary sequence (PRBS) signal with a switching rate of 147ms. Both signals were low-pass filtered with a 4<sup>th</sup> order Butterworth filter at 40Hz, and scaled to have a standard deviation of 0.0089 rad.

## D. Data analysis

The measured voluntary time-varying torque applied by the participants is needed to ensure time-varying joint properties, but is not relevant for the estimators. For this reason the 0.5Hz time-varying voluntary torque was removed by fitting and subtracting a low-frequency polynomial function, before performing system identification. The measured output and output used for identification are displayed in Fig. 13. All data were decimated to 128Hz before performing system identification.

The EMG data was high-pass filtered at 20Hz using a 2<sup>nd</sup> order filter. Then the signal was rectified followed by a 2<sup>nd</sup> order low-pass filter at 20Hz. Both filters were zero-phase digital filters.

## E. Results of experimental study human joint

The MVC of the participants was  $41.6 \pm 7.2$  Nm. Position and torque data are presented in Fig. 13 for both perturbations. The mean and standard deviation of the torque are presented at the bottom of Fig. 13. The torque data shows the voluntary torque applied by the participant on top of the torque in response to the perturbations. For a representative participant the mean standard deviations of the measured output torque of the FGWN and PRBS signals were 1.91 Nm and 3.30 Nm, respectively, showing more variability in the force produced for the PRBS perturbation. The participants reported that for the trials with PRBS signal it was harder to track the voluntary torque.

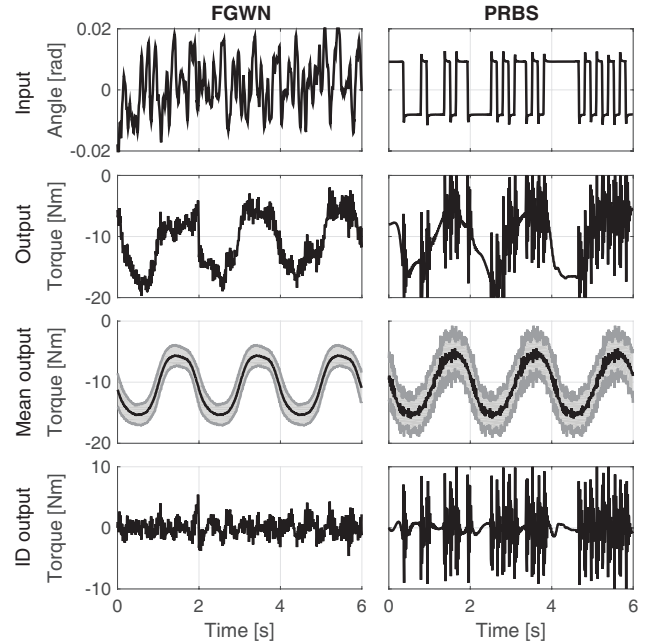


Fig. 13. The input and output represent the measured input and output, respectively. The mean output shows the mean and standard deviation of the output signal. The ID output shows the output of which the voluntary component has been removed, and which has been used for identification.

The estimated stiffness by each algorithm for both perturbation signals is presented in Fig. 14. The bottom figures show the mean and STD normalized EMG of the gastrocnemius.

Intrinsic stiffness is known to increase with contraction levels [9]. For this reason it is expected that the estimated stiffness would have a similar trend as the normalized EMG signal. The eIRF, bIRF, SDS, ESM, and mESM show this similar trend, especially visible for the FGWN perturbation, albeit with different offsets. The KBR shows the same frequency of varying stiffness with changing amplitudes.

The normalized EMG signal for the PRBS perturbations has a higher standard deviation of 17.4% compared to the FGWN perturbation 12.6%. This is similar to the torque measurements and the estimated stiffness, as can be seen from the bottom row of Fig. 15 where six out of seven algorithms have a higher mean standard deviation of the estimated stiffness.

The top row of Fig. 15 shows the mean of the estimated stiffness. The estimated stiffness was first averaged over 100 seconds of data and then averaged over the participants, for each algorithm. The top figures show little variation in mean estimated stiffness between participants, meaning that the participants had a similar ankle stiffness. The bottom row of Fig. 15 shows the standard deviation of the estimated stiffness. The standard deviation was first calculated for 100 seconds of data and then averaged over the participants. The bottom figures show that for the PRBS signal the estimated stiffness has a higher variance.

#### F. Main observations of experimental study human joint

- For the PRBS perturbation the measured torque output, normalized EMG signal, and estimated stiffness have a larger standard deviation.
- The LPV method does not show a similar trend as the EMG signal.
- The KBR has the same frequency as the normalized EMG trend, with varying amplitudes.
- The stiffness estimate with the short data segment methods (SDS, mESM, and ESM) and ensemble methods (eIRF and bIRF) all have the same trend similar to the EMG signal, with different offsets.
- The stiffness estimated with the short data segment methods overlap.
- The standard deviation of the mean estimated stiffness over participants is relatively low, meaning that the stiffness does not vary much between participants.

## VI. DISCUSSION

The objective of this study was to compare seven time-varying identification methods on their ability to estimate joint impedance.

#### A. Signal-to-noise ratio

In the simulation study the stiffness estimates of all methods, except the LPV method, improved with a higher SNR. It is as expected that the methods are able to achieve a more accurate estimate when less noise is present. The fact that this is not the case for the LPV method indicates that the method suffers from a bias.

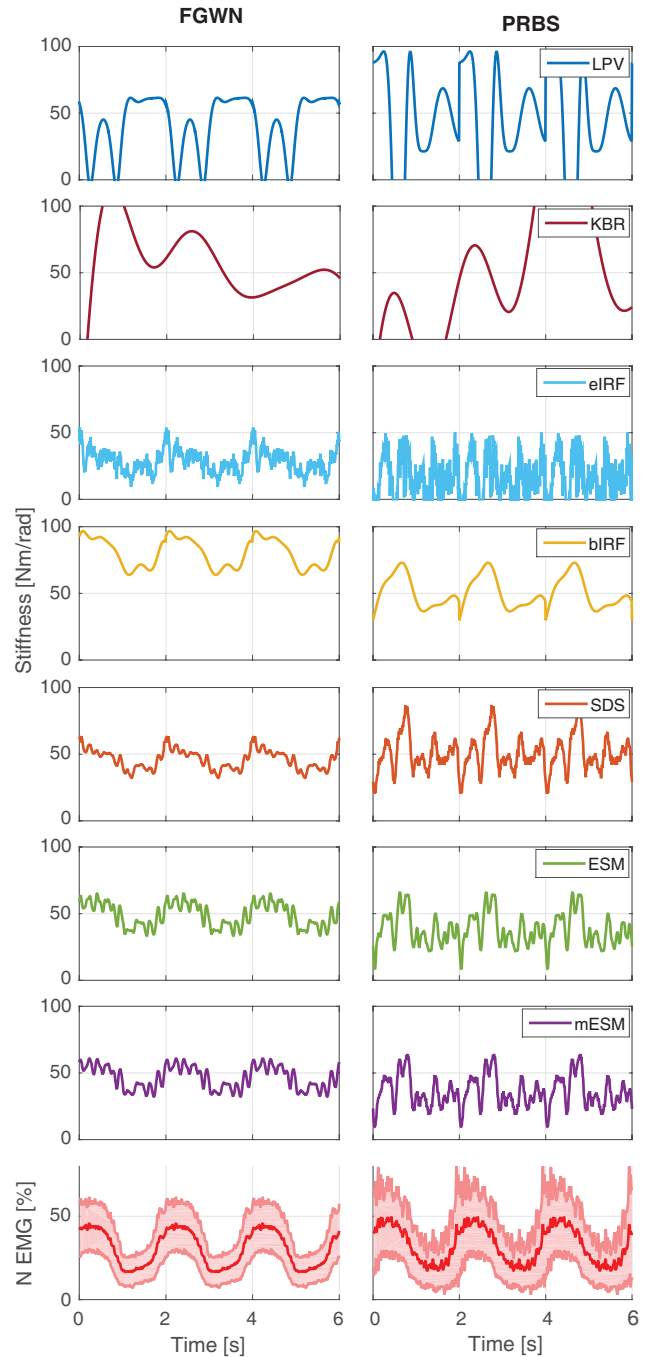


Fig. 14. Visual representation of the estimated stiffness by each system identification algorithm. The LPV and KBR are estimated using 100 seconds of data, the other algorithms using 400 seconds of data. The bottom figures show the EMG signal of the gastrocnemius muscle, where the solid red trace shows the mean of the signal and the red area shows the standard deviation of the signal.

The method that suffered most from a low SNR is the KBR. Reason for this is that the method does not make any assumptions on repetitions, either through a scheduling variable or ensemble averaging. The method therefore has the highest benefit from a higher SNR.

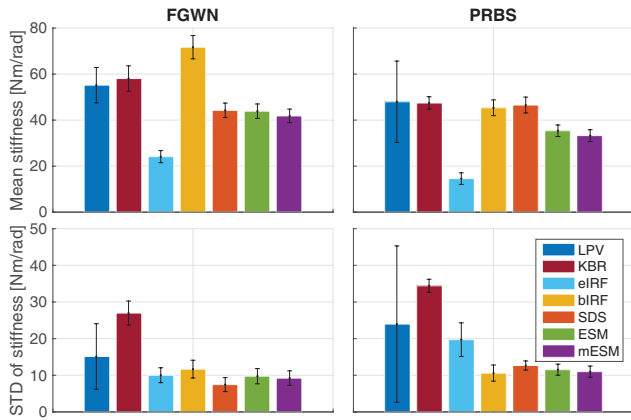


Fig. 15. Top row: The bars show the mean estimated stiffness over 100 seconds of data averaged over participants and the error bars show the standard deviation of this mean estimated stiffness over the participants. Bottom row: The bars show the standard deviation of estimated stiffness over 100 seconds averaged over participants and the error bars show the standard deviation of this mean standard deviation of the estimated stiffness of the participants.

### B. Number of samples

The estimates for both the ensemble (eIRF and bIRF) and short data segment (SDS, ESM, and mESM) methods improved when using more data both in simulation as for the mechanical experiment. This is in accordance with the expectations, as the methods have more realizations over which can be averaged and thus reduce the effect of noise.

The LPV and KBR did not improve when used with more data. For the KBR method this can be explained by the absence of a scheduling function or ensemble data. The effect of noise cannot be removed when used with more data. This is an advantage and a disadvantage as it will provide a constant estimate for more and less samples.

The LPV method, however, was expected to have a more accurate estimate of the stiffness when more data is used. By exploiting the scheduling variable it should be able to reduce the effect of noise. In the simulation study the LPV method was given perfect scheduling variables, being the normalized shape of the time-varying stiffness and damping. The estimate of the stiffness moved away from the true value when the algorithm was given more samples, similar as for the increased SNR. This combined information indicates that the method suffers from a bias. In the mechanical study the position of the rotational point was given as the scheduling function. Similar behaviour to the simulation study was found, with more data the estimate of the stiffness did not converge to the true value.

The eIRF is able to make the most accurate result being able to track abrupt time variations. However, the method requires hundreds of repetitions to achieve this. In the simulation study and the mechanical study the eIRF method requires around 200 repetitions to achieve the same error as the bIRF and short data segment methods with 25 to 50 repetitions. However, this is observed during a case where all realizations perfectly aligned. While experimenting on human subjects the realizations vary considerably. During human experiments the bIRF and short data segment methods require between 200 and 400 repetitions of the same movement to make a reasonable estimate, and the eIRF a few hundred more.

Alignment methods exist to reduce the amount of repetitions needed [28].

### C. Time-variation

The shape of the time-varying properties of the system had an effect on the ability of the algorithms to estimate the stiffness. In the simulation study the algorithms that result in more smooth estimates, being the SDS, ESM, mESM, bIRF, and KBR, had more trouble estimating the abruptly changing stiffness, where the KBR method was considered too smooth. The LPV method experienced influence of the damping scheduling variable, causing the estimated stiffness to incorrectly incorporate the shape of the damping.

For the mechanical system, the ability to estimate the stiffness of the algorithms changed for different time-variations. Most notable is that for the 0.5Hz sine time-variation the error was the highest for 5 algorithms for PRBS and 6 algorithms for FGWN perturbations. This is not in correspondence with the expectation that a slow time-variation is easier to track. An explanation can be found in the order in which the experiments were conducted. The first experiments done were the time-varying 0.5Hz sine wave for both the PRBS and FGWN perturbations. Then some trials not described in this study were performed. Then the time-varying experiments were conducted in the following order; 1Hz sine PRBS, 1Hz sine FGWN, 2Hz sine FGWN, 2Hz sine PRBS, 0.5Hz square PRBS, 0.5Hz square FGWN. After the time-varying trials, the time-invariant trials were conducted from which the true stiffness was calculated. It could be that during the trials in between the system changed, for example the friction of the lead screw changed or a bolt loosened, effectively changing the stiffness of the device. This could explain the inconsistent results of the 0.5Hz sine wave time-variation.

Following the same reasoning the results from the 0.5Hz square time-variation should have the smallest error, as the time-invariant trials were performed immediately after. The results confirm this by showing the best results for 5 of the 7 algorithms.

In the human study the participants were asked to vary the contraction of their ankle to induce a time-variation. The estimated stiffness was expected to follow a similar trend as the recorded EMG signal, as intrinsic stiffness varies with contraction levels [9]. The results from the human study confirm this by showing a similar trend for 5 of the algorithms. The effect is most pronounced for the FGWN perturbation type, presented in Fig. 16. The figure shows that the short data segment methods (SDS, ESM, and mESM) are very close together. The eIRF and bIRF have an offset from the short data segment methods. Which of the algorithms is closest to the true value remains unknown as well as the reason for the offset.

### D. Perturbation signal

In the simulation study the results for the FGWN and PRBS perturbation were similar. The median error for the multisine perturbation however was the highest for all algorithms. Reason for this could be that the signal did not contain enough higher frequencies for the algorithms to produce accurate results, or due to the periodicity of the signal.

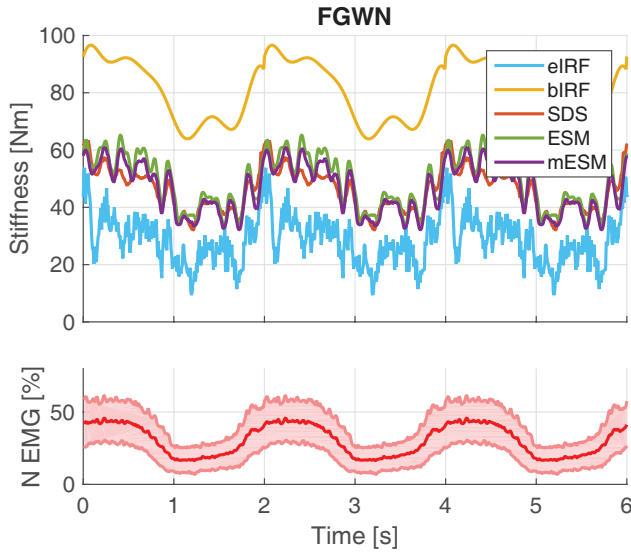


Fig. 16. Top figure is a visual representation of the estimated stiffness in the human experimental study using FGWN perturbations. Bottom figure represents the normalized EMG signal of the gastrocnemius muscle.

For the mechanical system all methods had a lower median error for the estimated stiffness when used with a FGWN perturbation compared to the PRBS perturbation. This can be attributed to the fact that the input signals had a different mean and standard deviation. Surprising is that the FGWN input had a lower standard deviation than the PRBS input, effectively giving the trials with a PRBS input the benefit of a higher SNR.

For the human study the FGWN and PRBS perturbations did have an equal mean and standard deviation, but produced different results. All participants reported that they found it more difficult to track the desired torque trajectory for the trials with the PRBS perturbation. The EMG and measured torque signals confirm this by showing a higher variance for the PRBS perturbation. The estimated stiffness also shows smoother time-varying behaviour for the FGWN perturbations. Reason for this is that due to the more abrupt PRBS perturbations a stronger response of the muscle was triggered causing a higher stiffness. The means of the estimated stiffness for the different perturbations signals, however, are quite similar.

The different ranges of the true stiffness of the mechanical system for the two perturbation signals had an effect on the results. The error is scaled to the RMS of the true stiffness, which is lower for the PRBS perturbation than the FGWN perturbation. The absolute error could be smaller while the percentage error would be larger when comparing between perturbation signals, creating a bias in the results.

#### E. True stiffness of the mechanical system

When looking at the results of the true stiffness in Fig. 8 it can be seen that the stiffness estimated using the FGWN and PRBS perturbations are different. This difference can be attributed to multiple causes. The main cause for the differences is the fact that the system is highly nonlinear, as the connections and bearings have some play allowing for some movement, rotation, and bending of the rotational point.

The different properties of the two perturbation signals, such as amplitude, mean, and standard deviation, combined with the nonlinearity of the system cause the springs to extend differently for both signals and thus have a different stiffness.

#### F. Limitations

A limitation for the simulation study is the fact that it uses ensemble data that is perfectly lined up. The dynamics of the simulated system are exactly the same for each realization, something that is not possible when experimenting on humans. Even when the time-variation is imposed on a human subject, the contractions and reflexes will never be the exact same [29]. This results in an advantage for the ensemble and short data segment methods and allows them to achieve better estimates than they would with real experimental data. To allow for a more fair comparison between ensemble and non-ensemble methods the dynamics of the model could be randomly changed and the phase could randomly shift for each realization.

A limitation of the variable stiffness device study is that the true stiffness is approximated by interpolating the results of time-invariant trials. It could be argued that the dynamics of a system are different under static and dynamic conditions.

Furthermore, for the mechanical system, the time-variations were computer controlled. This resulted, similar to the simulation study, in the dynamics of the system to be similar for each realization, again giving the ensemble and short data segment methods a slight advantage.

For the human study the PRBS perturbations were experienced as being too fierce by the participants, and they had trouble following the desired trajectory. This may have caused a more variable response to the perturbations and the estimations may not be as accurate. However, the PRBS perturbations had the same standard deviation as the FGWN perturbation which the participants were able to reject properly. This would indicate that the FGWN perturbations are preferable as a higher SNR can be achieved with this perturbation signal when experimenting on humans.

#### G. Methods

The LPV method appears to have a bias in both the simulation and mechanical study as the estimated stiffness moved away from the true value with an increased SNR and more samples. For the human study the estimated stiffness does not follow the same trend as the measured EMG signal, even though this was expected. This could be caused by the fact that the underlying scheduling variable is hard to measure, and the EMG signal of just one muscle was measured.

The eIRF method was able to achieve a low error and converge to the true stiffness and track fast changes, for both the simulation study and mechanical study. It however needs hundreds of realizations of the same movement to do so.

The bIRF method was able to estimate the stiffness with the lowest error for both the simulation study and mechanical study with a FGWN perturbation. The algorithms is able to achieve reasonably low errors for PRBS perturbations.

The SDS method is most robust as it was able to structurally achieve low errors in the estimated stiffness for all perturbation signals in both the simulation study and mechanical study.

The mESM and ESM methods are very similar and generally able to achieve good results. However, the ESM is structurally able to achieve lower errors than the mESM for both the simulation study and mechanical study. In simulation the methods are able to achieve good results for all perturbation signals, but during the mechanical study the error of the estimated stiffness for the FGWN perturbation were much lower.

The KBR method has the highest overall error for both the simulation study and the mechanical study. For the FGWN perturbation the method was generally able to track the frequency of the time-variation. Reason for the relatively poor results could be that the identification parameters can be tuned, while in this study the algorithm was left to decide the value of the  $\gamma$  parameter. Furthermore, the method allows for the use of Leave-two-out (LTO) cross validation [21] possibly enhancing the results found in this paper.

## VII. CONCLUSIONS

Seven algorithms were used and tested to compare their ability to estimate joint stiffness using three data sets. A simulation study, an experimental study on a mechanical device with a known true stiffness, and an experimental study on human ankles.

From the simulation study it became clear that the algorithms had better performance using the FGWN and PRBS perturbation signals, compared to the multisine perturbation signal. For the mechanical study the true stiffness was estimated, but appeared to vary between perturbation signals, because the device is nonlinear. Overall the FGWN perturbations resulted in lower estimation errors compared to the PRBS signal.

Following the results of the simulation and mechanical study it was found that the SDS method was most robust by structurally estimating the stiffness with low error. The bIRF was able to estimate the stiffness with the lowest error when FGWN perturbations were used. The LPV appears to suffer from a bias. The mESM and ESM methods are very similar to each other, but the ESM method was structurally able to estimate with lower errors compared to the mESM method. The KBR method structurally estimated with higher errors compared to the other methods, but might be able to get better results when tuned better and using LTO cross validation.

During the human study the participants found the PRBS signal to be too forceful, which was also visible in the results. The torque measurements and EMG signal, for the PRBS perturbations, had a higher variance which could also be seen in the estimated stiffness. The results for the FGWN perturbation were smoother. The SDS, mESM, ESM, bIRF and eIRF methods followed the same trend as the normalized EMG signal, albeit with an offset between the methods. The reason for the offset is unknown, and because the true underlying values of the human stiffness is not known, there is no way to know which method is correct.

When the time-varying realizations are perfectly lined up, the eIRF can make a reasonable estimate using 200 repetitions. The bIRF and short data segment methods can achieve a similar result with around 50 repetitions of the same movement. However, humans are generally incapable of producing this many perfectly lined up repetitions. In order to achieve reasonable results the bIRF and short data segment methods require between 200 and 400 repetitions, where the eIRF requires hundreds more.

In order to advance and evaluate the system identification algorithms for identifying joint impedance the evaluation procedure should be standardized. This includes the availability of simulation data, a mechanical system with known values, and the standardization of experimental procedures on human joints. This allows for the comparison of algorithms and demonstrate the strengths and weaknesses of each algorithm.

## REFERENCES

- [1] Robert E Kearney, Richard B Stein, and Luckshman Parameswaran. Identification of intrinsic and reflex contributions to human ankle stiffness dynamics. *IEEE transactions on biomedical engineering*, 44(6):493–504, 1997.
- [2] Alfred Christiaan Schouten. Proprioceptive reflexes and neurological disorders. 2004.
- [3] Elliott J Rouse, Levi J Hargrove, Eric J Perreault, and Todd A Kuiken. Estimation of human ankle impedance during the stance phase of walking. *Ieee Transactions On Neural Systems And Rehabilitation Engineering*, 22(4):870–878, 2014.
- [4] Daniel Ludvig and Eric J Perreault. Task-relevant adaptation of musculoskeletal impedance during posture and movement. In *American Control Conference (ACC), 2014*, pages 4784–4789. IEEE, 2014.
- [5] Serge M Pfeifer. *Biomimetic stiffness for transfemoral prostheses*. PhD thesis, ETH Zurich, 2014.
- [6] Kevin H Ha, Huseyin Atakan Varol, and Michael Goldfarb. Volitional control of a prosthetic knee using surface electromyography. *IEEE Transactions on Biomedical Engineering*, 58(1):144–151, 2011.
- [7] Eric Perreault, Levi Hargrove, Daniel Ludvig, Hyunglae Lee, and Jon Sensinger. Considering limb impedance in the design and control of prosthetic devices. In *Neuro-Robotics*, pages 59–83. Springer, 2014.
- [8] Winfred Mugge, David A Abbink, Alfred C Schouten, Julius PA Dewald, and Frans CT Van Der Helm. A rigorous model of reflex function indicates that position and force feedback are flexibly tuned to position and force tasks. *Experimental brain research*, 200(3-4):325–340, 2010.
- [9] MM Mirbagheri, H Barbeau, and RE Kearney. Intrinsic and reflex contributions to human ankle stiffness: variation with activation level and position. *Experimental Brain Research*, 135(4):423–436, 2000.
- [10] Frans CT Van der Helm, Alfred C Schouten, Erwin de Vlugt, and Guido G Brouwn. Identification of intrinsic and reflexive components of human arm dynamics during postural control. *Journal of neuroscience methods*, 119(1):1–14, 2002.
- [11] MTV Johnson, AN Kipnis, MC Lee, and TJ Ebner. Independent control of reflex and volitional emg modulation during sinusoidal pursuit tracking in humans. *Experimental brain research*, 96(2):347–362, 1993.
- [12] RB Stein and RE Kearney. Nonlinear behavior of muscle reflexes at the human ankle joint. *Journal of neurophysiology*, 73(1):65–72, 1995.
- [13] Martijn Kerklaan. Linear parameter system identification for joint impedance. 2018.
- [14] Mahsa A Golkar, Ehsan Sobhani Tehrani, and Robert E Kearney. Linear parameter varying identification of dynamic joint stiffness during time-varying voluntary contractions. *Frontiers in computational neuroscience*, 11:35, 2017.
- [15] Kian Jaleleddini, Mahsa A Golkar, and Robert E Kearney. Measurement of dynamic joint stiffness from multiple short data segments. *IEEE Transactions on Neural Systems and Rehabilitation Engineering*, 25(7):925–934, 2017.

- [16] Diego L Guarin and Robert E Kearney. Identification of a time-varying, box-jenkins model of intrinsic joint compliance. *IEEE Transactions on Neural Systems and Rehabilitation Engineering*, 25(8):1211–1220, 2017.
- [17] Diego L Guarin and Robert E Kearney. Estimation of time-varying, intrinsic and reflex dynamic joint stiffness during movement. application to the ankle joint. *Frontiers in computational neuroscience*, 11:51, 2017.
- [18] Daniel Ludvig and Eric J Perreault. System identification of physiological systems using short data segments. *IEEE Transactions on Biomedical Engineering*, 59(12):3541–3549, 2012.
- [19] Gaia Cavallo. Skirt decomposition method for the identification of linear time-varying human joint admittance. 2017.
- [20] Michel Verhaegen and Vincent Verdult. *Filtering and system identification: a least squares approach*. Cambridge university press, 2007.
- [21] John Lataire, Rik Pintelon, Dario Piga, and Roland Tóth. Continuous-time linear time-varying system identification with a frequency-domain kernel-based estimator. *IET Control Theory & Applications*, 11(4):457–465, 2016.
- [22] J Bart MacNeil, RE Kearney, and IW Hunter. Identification of time-varying biological systems from ensemble data. *IEEE Trans. Biomed. Eng.*, 39(12):1213–1225, 1992.
- [23] Jan-Willem Van Wingerden and Michel Verhaegen. Subspace identification of bilinear and lpv systems for open-and closed-loop data. *Automatica*, 45(2):372–381, 2009.
- [24] Michel Verhaegen. A subspace model identification solution to the identification of mixed causal, anti-causal lti systems. *SIAM Journal on matrix analysis and applications*, 17(2):332–347, 1996.
- [25] Fredric J Harris. On the use of windows for harmonic analysis with the discrete fourier transform. *Proceedings of the IEEE*, 66(1):51–83, 1978.
- [26] David J Thomson. Spectrum estimation and harmonic analysis. *Proceedings of the IEEE*, 70(9):1055–1096, 1982.
- [27] Erwin de Vlugt, Alfred C Schouten, and Frans CT van der Helm. Closed-loop multivariable system identification for the characterization of the dynamic arm compliance using continuous force disturbances: a model study. *Journal of neuroscience methods*, 122(2):123–140, 2003.
- [28] Daniel Ludvig and Eric J Perreault. The dynamic effect of muscle activation on knee stiffness. In *Engineering in Medicine and Biology Society (EMBC), 2014 36th Annual International Conference of the IEEE*, pages 1599–1602. IEEE, 2014.
- [29] Christopher M Harris and Daniel M Wolpert. Signal-dependent noise determines motor planning. *Nature*, 394(6695):780, 1998.
- [30] M Lortie and RE Kearney. Identification of physiological systems: estimation of linear timevarying dynamics with non-white inputs and noisy outputs. *Medical and Biological Engineering and Computing*, 39(3):381–390, 2001.

## VIII. APPENDIX

### A. Time-varying system identification methods

1) *LPV*: The non-causal LPV subspace identification method has the following form:

$$x_{k+1}^c = A_k x_k^c + B_k^c u_k + K_k^c y_k \quad \text{causal part,} \quad (8)$$

$$E_k x_{k+1}^{ac} = x_k^{ac} - B_k^{ac} u_k - K_k^{ac} y_k \quad \text{anti-causal part,} \quad (9)$$

$$y_k = [C^c \quad C^{ac}] \begin{bmatrix} x_k^c \\ x_k^{ac} \end{bmatrix} + D u_k + e_k \quad (10)$$

where the superscripts  $c$  and  $ac$  indicate the causal and anti-causal part, respectively,  $u_k$  is the input,  $y_k$  is the output,  $x_k$  is the state,  $e_k$  is the innovation sequence,  $k$  is the time step, and  $E_k, A_k, B_k, K, C$ , and  $D$  are the system matrices of the generalized state space description. Note that  $E_k, A_k, B_k^{ac}$ , and  $B_k^c$  are time-varying.

$$E_k = \sum_{i=1}^m \mu_k^{(i)} E^{(i)} \quad (11)$$

$$\mu_k = \begin{bmatrix} 1 & \mu_k^{(2)} & \dots & \mu_k^{(m)} \end{bmatrix}^T \quad (12)$$

where  $\mu_k$  is the scheduling variable consisting of  $m$  local models. The identification procedure for identifying the system matrices is beyond the scope of this paper and details can be found in [13].

2) *eIRF*:

$$y(i) = \Delta t \sum_{j=M_1}^{M_2} u(i-j) h(t, j) \quad (13)$$

where  $y$  is the output,  $u$  is the input,  $h$  is the impulse response function,  $i$  is the sample time,  $j$  is the lag of the impulse response function,  $\Delta t$  is the sampling increment, and  $M_1$  and  $M_2$  are the maximum and minimum lag, respectively [18]. The IRF  $h(t, j)$  can be computed as follows:

$$h(t, j) = \Delta t^{-1} \Phi_{xx}^{-1} \Phi_{xy} \quad (14)$$

where

$$\Phi_{xy} = [\phi_{xy}(t, M_1) \quad \dots \quad \phi_{xy}(t, M_2)] \quad (15)$$

and

$$\Phi_{xx} = \begin{bmatrix} \phi_{xx}(t-M_1, 0) & \dots & \phi_{xx}(t-M_2, M_1-M_2) \\ \vdots & \ddots & \vdots \\ \phi_{xx}(t-M_1, M_2-M_1) & \dots & \phi_{xx}(t-M_2, 0) \end{bmatrix} \quad (16)$$

where

$$\phi_{xy}(t, k) = \frac{1}{R} \sum_{r=1}^R x(t-k, r) y(t, r) \quad (17)$$

where  $r$  is the realization number and  $R$  the total number of realizations.

More details about this method can be found in [30].

3) *bIRF*:

$$\theta(i) = \theta_0(i) + \theta_p(i) \quad (18)$$

where  $\theta_0(i)$  is the movement trajectory and  $\theta_p(i)$  is the position perturbation.

$$TQ(i) = TQ_0 + TQ_p(i) \quad (19)$$

where  $TQ_0$  is a constant torque, produced by passive mechanisms due to  $\theta_0$ , and by active mechanisms due to the constant muscle activation.  $TQ_p(i)$  is a perturbation torque, produced by the excitation of intrinsic and reflex mechanisms given by

$$TQ_p(i) = TQ_I(i) + TQ_R(i) + TQ_\Delta(i) \quad (20)$$

where  $TQ_I(\text{tk})$  and  $TQ_R(\text{tk})$  are the torques produced by the intrinsic and reflex mechanisms, which cannot be measured directly.

where  $TQ(\text{tk})$  is an additional torque due to difference in passive and voluntary torques during the perturbed and unperturbed experiments.

$$TQ_I(i) = \sum_{\tau=-L}^{\tau=L} h_I(\tau, i) \theta_p(i - \tau) \quad (21)$$

The TV IRF will be approximated by a linear combination of basis functions as

$$h_I(\tau, i) = \sum_{j=0}^{j=n_\lambda} \lambda_{\tau, j} \Lambda_j(i) \quad (22)$$

where  $\{\lambda_j(i)\}_{j=0}^{j=n_\lambda}$  are a set of time-varying basis functions and  $\lambda_{\tau, j}$  the corresponding coefficients.

The reflexive component was not taken into consideration in this paper.

More details about this method can be found in [17].

4) *SDS*: It is calculated the exact same way as the Ensemble IRF by Robert Kearney, except for the different calculation of auto- and cross-correlation:

$$\phi_{xy}(t, k) = \frac{1}{NR} \sum_{r=1}^R \sum_{i=t-N/2}^{i=t+N/2} x(i-k, r) y(i, r) \quad (23)$$

where  $t$  is the time in the middle of each short data segment and  $N$  number of samples in each segment.

More details about this method can be found in [18].

5) *ESM & mESM*: The FRF is calculated using the mean spectral densities.

$$H(k) = \frac{\bar{S}_{yu}(k)}{\bar{S}_{uu}(k)} \quad (24)$$

Where  $H(k)$  is the FRF at time-step  $k$ ,  $k = L/2 \dots N - L/2$  where  $L$  is the size of the window,  $\bar{S}_{yu}(k)$  is the mean cross-spectral density, and  $\bar{S}_{uu}(k)$  is the mean auto-spectral density calculated using equation (25).

$$\bar{S}_{yu}(k) = \frac{1}{L} \sum_{i=-L/2}^{L/2} S_{yu}(k+i) \quad (25)$$

where  $S_{yu}(k)$  is the cross-spectral density at time-step  $k$ .

$$S_{yu}(k) = \frac{1}{L} Y_h(k) U_h(k)^* \quad (26)$$

where  $U_h$  and  $Y_h$  are the Fourier transforms of each realization of the input  $u_h$  and output  $y_h$ , respectively, to which a Hanning windows has been applied.

$$y_h(k) = \begin{bmatrix} y_1(k - \frac{L}{2}) & \dots & y_1(k + \frac{L}{2}) \\ \vdots & \ddots & \vdots \\ y_n(k - \frac{L}{2}) & \dots & y_n(k + \frac{L}{2}) \end{bmatrix} \circ [w(k - \frac{L}{2}) \quad \dots \quad w(k + \frac{L}{2})] \quad (27)$$

where  $y_n$  is the output of realization  $n$ , and  $w$  is the Hanning window computed using equation (28).

$$w(k) = \frac{1}{2} (1 - \cos(\frac{2\pi k}{L-1})) \quad (28)$$

6) *KBR*: The system's input and output signals,  $u(t)$  and  $y(t)$ , are assumed to satisfy the linear differential equation:

$$y(t) = - \sum_{n=1}^{N_a} a_n(t) \frac{d^n y(t)}{dt^n} + \sum_{n=0}^{N_b} b_n(t) \frac{d^n u(t)}{dt^n} \quad (29)$$

where  $a_n(t)$  and  $b_n(t)$  are the time-varying coefficients which are smooth functions of  $t$ . These coefficients are estimated via kernel-based regression. In essence, the estimate is defined as the following minimizer:

$$\hat{a}_n, \hat{b}_n = \operatorname{argmin}_{k \in \mathbb{K}_{\text{int}}} \sum \frac{|E(k, a_n, b_n)|^2}{\hat{\sigma}_E^2(k, a_n, b_n)} + \sum_{n=1}^{N_a} a_n^T K^{-1} a_n + \sum_{n=0}^{N_b} b_n^T K^{-1} b_n \quad (30)$$

where  $E$  is the DFT of the equation error (the difference between the left and right hand side of (29)), evaluated in  $\mathbb{K}_{\text{int}}$ , the bins corresponding to the frequency band of interest.

$a_n$  and  $b_n$  are obtained by vectorising  $a_n(t)$  and  $b_n(t)$  in  $t = 0, T_s, \dots, (N-1)T_s$ . Note that (30) is a non-quadratic (and in general non-convex) problem, due to the division by  $\hat{\sigma}_E$ . This is solved via an iterative convex relaxation, where  $\hat{\sigma}_E$  initialized to 1 and, for the  $m^{\text{th}}$  iteration, is computed as  $\hat{\sigma}_{E,m}^2(k) \leftarrow \hat{\sigma}_{E,m}^2(k, \hat{a}_{n,m}, \hat{b}_{n,m})$ , with  $\hat{a}_{n,m-1}, \hat{b}_{n,m-1}$  the estimates obtained at the  $(m-1)^{\text{th}}$  iteration. The kernel matrix  $K$  is semi-positive definite and symmetric, and imposes structure on the estimated parameters.  $K$  is obtained from the squared exponential radial basis function:

$$K(t, t') = \gamma e^{-\frac{(t-t')^2}{\sigma^2}}, \quad t, t' = 0, T_s, \dots, (N-1)T_s \quad (31)$$

In which  $\sigma$  determines the smoothness of the estimated time-varying coefficients.  $\gamma$  represents the inverse of the amount of regularisation applied, defining a bias versus variance trade-off of the estimated coefficients. Details can be found in [21].

### B. Extraction and mapping of true stiffness of mechanical variable stiffness device

To assess the stiffness estimates of the time-varying system identification algorithms, the true stiffness of the device was extracted. Five time-invariant trials at different positions of the rotational point were performed for both perturbations. The stiffness was then estimated using a time-invariant system identification method for each point. A quadratic curve was then fitted to these points to create a mapping for the whole range of motion of the rotational point. This was done for both FGWN and PRBS perturbations.

1) *Time-invariant trials*: Each time-invariant trial lasted for 60 seconds and was sampled at 2500Hz. For the PRBS signal an amplitude of 5mm and a switching rate of 147ms was used. The FGWN signal was low pass filtered using a 2<sup>nd</sup> order Butterworth filter at 5Hz and had a standard deviation of 2mm. Both signals were low pass filtered using a 4<sup>th</sup> order Butterworth filter at 40Hz.

2) *Stiffness calculation*: The stiffness was extracted by estimating the frequency response function for each trial.

$$\hat{H}_{yu}(f) = \frac{\hat{S}_{yu}(f)}{\hat{S}_{uu}(f)} \quad (32)$$

where  $\hat{H}_{yu}(f)$  is the estimated frequency response function, and  $\hat{S}_{yu}(f)$  and  $\hat{S}_{uu}(f)$  are the cross- and auto-spectral densities, respectively. The spectral densities are calculated as follows:

$$\hat{S}_{yu}(f) = \frac{1}{N} Y(f) U^*(f) \quad (33)$$

where  $Y(f)$  is the Fourier transform of the output signal  $y(t)$ ,  $U^*(f)$  is the complex conjugate of the Fourier transform of the input signal  $u(t)$ , and  $N$  is the number of samples used for identification.

The stiffness was then determined by calculating the static gain for each trial. The static gain was calculated by averaging over the magnitudes between 0.1 and 2.5Hz of the estimated FRF. The stiffness was expected to change quadratically with the position of the rotational point, because whenever the rotational point moves the part removed from the moment arm on one side gets added to moment arm on the other side, causing the ratio to shift quadratically, Equation (34).

$$K_1 = \frac{(r - r_1)^2}{r_1^2} K_2 \quad (34)$$

where  $K_1$  is the stiffness at the point of perturbation,  $K_2$  is the true stiffness of the combined springs,  $r_1$  is length of the bar on the left of the rotational point, and  $r$  is the total length of the bar.

To create a mapping of the stiffness a quadratic function was estimated to interpolate between the results of the static trials. Fig. 17 displays the results from the estimated and theoretical stiffness.

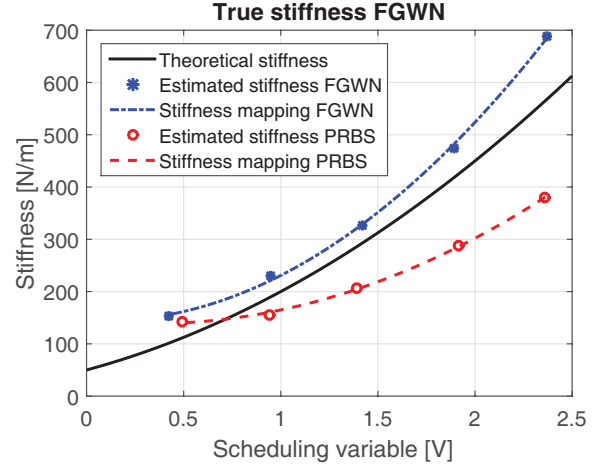


Fig. 17. Theoretical and estimated stiffness interpolated between time-invariant trials for both FGWN and PRBS perturbations.

### C. Identification parameters of time-varying methods

The parameters used for identification during the simulation study, mechanical experimental study, and human experimental study can be found in Table VI.

TABLE VI. PARAMETERS USED IN THE METHODS USED FOR SYSTEM IDENTIFICATION

<b>LPV</b>		
$P_{end}$	Maximum system order to optimize VAF	3
<b>KBR</b>		
$N_a$	Order of TV coefficient	1
$N_b$	Order of TV coefficient	3
$\sigma$	Smoothing parameter	Number of samples in 1 realization
$\gamma$	Hyperparameter to apply regularisation	Determined by the optimWLS function
<b>eIRF</b>		
$N_{lags}$	Number of lags to estimate IRF	4
<b>bIRF</b>		
$N_{lags}$	Number of lags to estimate IRF	4
$P_{max}$	Maximum number of iterations to optimize the VAF	3
<b>SDS</b>		
$N_{lags}$	Number of lags to estimate IRF	4
$N_{window}$	Number of samples over which the system averaged	10
<b>mESM</b>		
$N_w$	Spectral smoothing parameter	1
$L$	Range of window over which to optimize VAF	30...60
<b>ESM</b>		
$L$	Range of window over which to optimize VAF	30...60